

# ALL WHISTLERS ARE NOT CREATED EQUALLY: SCATTERING OF STRAHL ELECTRONS IN THE SOLAR WIND VIA PARTICLE-IN-CELL SIMULATIONS

Shinji Saito and S. Peter Gary  
Los Alamos National Laboratory  
Los Alamos, NM

13 September 2006

## Abstract

Solar wind observations show that suprathermal electrons ( $70 \text{ eV} \lesssim \text{Energy} \lesssim 1 \text{ keV}$ ) of the magnetic-field-aligned “strahl” component have broader pitch-angle distributions than are predicted by adiabatic theories of solar wind expansion. Magnetosonic-whistler fluctuations propagating toward the Sun at  $\mathbf{k} \times \mathbf{B}_o = 0$  (where  $\mathbf{B}_o$  is the background magnetic field) have a strong cyclotron resonance with suprathermal electrons propagating in the anti-Solar direction along  $\mathbf{B}_o$ . This resonance enables strong pitch-angle scattering; thus whistlers are a likely source of the observed strahl broadening. Particle-in-cell simulations in a magnetized, homogeneous, collisionless plasma of electrons and protons are used to study the response of a strahl-like electron component to whistler fluctuation spectra. If the whistler anisotropy instability is excited via the initial application of  $T_\perp/T_\parallel > 1$  to the electron core component, the resulting electron scattering leads to strahl pitch-angle distributions which decrease in width as electron energy increases. In contrast, if a power spectrum of whistler fluctuations proportional to  $k^{-3}$  is initially applied to the simulations, the resulting electron scattering leads to strahl pitch-angle distributions which increase in width as electron energy increases.

## 1. Introduction

In the solar wind near Earth, the relatively dense, relatively cool core electrons are strongly influenced by particle-particle collisions [*Phillips and Gosling, 1990*], so that the velocity distributions of this component are usually observed to be Maxwellian or bi-Maxwellian-like. Above about 70 eV, however, Coulomb collisions become so weak that suprathermal electron distributions can become distinctly non-Maxwellian. Because they are relatively collisionless, the suprathermals can be sensitive indicators of wave-particle processes in the solar wind. Computer simulations of such processes, as described here, can provide useful insights for observational studies of these electrons.

At energies from above 70 eV to about 1 keV, two distinct electron components have been identified: the halo and the strahl. Both components are quite tenuous compared

to the core [Maksimovic *et al.*, 2005], but they are very different in their velocity-space properties [Gosling *et al.*, 2001]. The halo is isotropic or nearly so [Feldman *et al.*, 1975], whereas the strahl is highly anisotropic [Rosenbauer *et al.*, 1977; Feldman *et al.*, 1978], appearing as a finger in velocity space pointing along the background magnetic field  $\mathbf{B}_o$  away from the Sun. The strahl, which is thought to consist of hot coronal electrons, has been scattered so that its pitch-angle widths are broader than that of the very narrow beam which is predicted by the adiabatic theory of solar wind expansion. The halo is usually interpreted as electrons which have been strongly scattered; the quasi-isotropic character of the halo requires that the scattering has taken place not only between the Sun and the Earth, but also at distances well beyond 1 AU [Gosling *et al.*, 2001]. But the specific scattering mechanisms of both strahl and halo remain unidentified [Maksimovic *et al.*, 2005].

Although most observations show that the strahl becomes more anisotropic [e.g., Feldman *et al.*, 1978, Lemons and Feldman, 1983; Pilipp *et al.*, 1987] or retains the same anisotropy [Hammond *et al.*, 1996] as electron energy increases, recent WIND spacecraft observations of Pagel *et al.* [2005] show that strahl pitch-angle distributions in the fast solar wind on average become somewhat broader with increasing electron energy. Vocks *et al.* [2005] also report WIND observations showing that suprathermal velocity distributions become more nearly isotropic at higher electron energies in the fast wind. Furthermore, Pagel *et al.* [2006] using observations from the ACE spacecraft showed that, for 29 suprathermal electron scattering events corresponding to enhanced levels of relatively high frequency magnetic fluctuations, the pitch-angle width of the strahl uniformly increased as the electron energy increased.

Suprathermal electrons have a cyclotron resonance with whistler fluctuations at  $\mathbf{k} \times \mathbf{B}_o = 0$ . In contrast, Alfvén-cyclotron fluctuations usually have damping which increases with wavenumber and do not attain the short wavelengths required for that resonance. Therefore, whistlers are the electromagnetic mode most likely to provide pitch-angle scattering of the suprathermals. Vocks and Mann [2003] and Vocks *et al.* [2005] used quasi-linear theory with a given power spectrum of magnetic fluctuations to show that whistlers can strongly pitch-angle scatter solar wind suprathermals, and that such scattering leads to an electron velocity distribution which becomes more isotropic with increasing energy. However, these calculations assumed a fixed, given power spectrum of whistler fluctuations; it is important to show these results also are present in the more physical self-consistent model represented by particle-in-cell simulations.

The source of enhanced whistlers determines the characteristics of their power spectrum, and it is the spectral properties that determine which electrons undergo wave-particle interactions, and how strongly they are scattered. There are at least three such sources: heat flux instabilities, core anisotropy instabilities, and wave-wave interactions. The first

of these is not a likely contributor to electron scattering near 1 AU because, as argued by *Pagel et al.* [2006], dispersion theory based upon electron observations predicts no significant growth for whistler heat flux instabilities. On the other hand, processes such as compression due to interplanetary shocks may drive  $T_{\perp}/T_{\parallel} > 1$  on the core (where the subscripts correspond to directions relative to  $\mathbf{B}_o$ ) [*Phillips et al.*, 1989]; this anisotropy can, in turn, excite the whistler anisotropy instability which may be the source of the enhanced whistler fluctuations observed downstream of such shocks [*Pierre et al.*, 1995; *Lengyel-Frey et al.*, 1996]. Section 2 describes a particle-in-cell simulation in which such fluctuations scatter the suprathermals.

Another potential source of enhanced whistlers are wave-wave interactions which lead, for example, to turbulent cascades and which, in turn, imply broadband power law magnetic fluctuation spectra in the whistler regime, such as have been observed by *Beinroth and Neubauer* [1981] and *Bale et al.* [2005]. Section 3 describes a second simulation in which a broadband spectrum is applied at  $t = 0$ , and the subsequent electron responses are computed.

We used a three-dimensional, fully relativistic, collisionless particle-in-cell electromagnetic simulation code [*Buneman*, 1993] to compute the results described below. For both runs described below, the system is essentially one-dimensional, with spatial dimensions  $L_x = 4096\Delta$ ,  $L_y = 3\Delta$  and  $L_z = 3\Delta$  where  $\Delta$  is the grid size. For both simulations, the time step is  $\delta t = 0.05/\omega_e$ , the grid spacing is  $\Delta = 0.10c/\omega_e$ , and the plasma is homogeneous with periodic boundary conditions, where the plasma frequency of the  $j$ th species is  $\omega_j \equiv \sqrt{4\pi n_j e_j^2/m_j}$ . Both simulations begin with three bi-Maxwellian electron components representing the core (subscript  $c$ ), the strahl ( $s$ ), and halo ( $h$ ). The subscript  $e$  represents overall electron properties, i.e.,  $n_e = n_c + n_s + n_h$ ,  $v_c$  represents the core thermal speed, and  $v_{oj}$  represents the magnetic-field-aligned average flow velocity of the  $j$ th component relative to the protons. We choose the following initial parameters:  $m_p/m_e = 1836$ ,  $\tilde{\beta}_{\parallel c} = 8\pi n_e k_B T_{\parallel c}/B_o^2 = 0.50$ ,  $n_c/n_e = 0.85$ ,  $n_s/n_e = 0.05$ ,  $n_h/n_e = 0.10$ ,  $v_{os}/v_c = -2.0$ ,  $v_{oh}/v_c = +0.0$ ,  $v_{oc} = -(n_s v_{os} + n_h v_{oh})/n_c$ ,  $T_{\parallel c}/T_{\parallel p} = 1.0$ ,  $T_{\parallel s}/T_{\parallel c} = 3.0$ ,  $T_{\parallel h}/T_{\parallel c} = 10$ ,  $T_{\perp c}/T_{\parallel c} = 3.0$  or  $1.0$ ,  $T_{\perp s}/T_{\parallel s} = 0.10$ , and  $T_{\perp h}/T_{\parallel h} = 1.0$ . Almost all of these parameters are consistent with typical observations in the solar wind near 1 AU. Untypical parameters include the relatively large strahl density, chosen to improve the suprathermal statistics, as well as the relatively large core anisotropy chosen in Section 2 and the relatively large initial fluctuation level used in Section 3, chosen to reduce computation time and to enhance the consequences of the scattering.

## 2. Simulation: Initially Anisotropic Electron Core

This section describes a simulation of the whistler anisotropy instability, an electromagnetic mode which is driven unstable by the condition  $T_{\perp e}/T_{\parallel e} > 1$ . For a

single, bi-Maxwellian electron velocity distribution, unstable modes typically arise at  $\omega_p/c \ll k < \omega_e/c$  and  $\Omega_p \ll \omega_r < |\Omega_e|$  [e.g., Fig. 7.7 of *Gary, 1993*], with maximum growth rate at  $\mathbf{k} \times \mathbf{B}_o = 0$ . Here the cyclotron frequency of the  $j$ th species is  $\Omega_j \equiv e_j B_o / m_j c$ . The electrons most strongly resonant with this instability are those with  $v_{\parallel}$  greater than the electron thermal velocity; a major consequence of this resonant interaction is pitch-angle scattering which reduces the overall anisotropy of the electron distribution [*Gary and Wang, 1996*].

The simulation described in this section begins with the three component electron distribution described above, with  $T_{\perp c} / T_{\parallel e} = 3.0$ . As a result the whistler anisotropy instability is excited and grows to saturation as illustrated in Figure 1a. Furthermore, Figure 1b shows that the spectrum of enhanced fluctuations lies within  $0.4 \lesssim kc/\omega_e \lesssim 0.9$ , as would be expected from linear theory, which predicts approximately the same range of unstable wavenumbers for these parameters.

Figure 2 illustrates the electron velocity distribution at both  $t = 0$  and  $|\Omega_e|t = 100.0$ . The instability is driven by the anisotropic core electrons, and it is those electrons which are most strongly scattered; the sense of the scattering, as it typically is for such an incoherent process, is down the gradient of the velocity distribution along a curve of constant energy in the wave frame. The result is to reduce the core anisotropy, as shown in the late-time panel. Low-energy strahl electrons are also resonant with and scattered by the enhanced fluctuations; but for this component the gradient on the velocity distribution points from smaller to larger  $v_{\perp}$  so that, as shown in Figure 2b, this part of the strahl has a broadened pitch-angle distribution at late times.

This effect is shown more clearly in Figure 3, which illustrates the electron pitch-angle distributions for three values of  $v$  at initial and late times. The less energetic electrons are more strongly resonant with the relatively short-wavelength enhanced fluctuations and are therefore scattered more strongly; in both cases the scattering is down the gradient of the velocity distribution, so that the consequence is to reduce the anisotropies of both the core and the strahl. The weakening of the resonance at larger  $v$  means that the strahl retains its initial narrow character with increasing electron energy.

### 3. Simulation: Initial Enhanced Fluctuation Spectrum

The simulation described in this section begins with an isotropic core distribution, i.e.,  $T_{\perp c} / T_{\parallel e} = 1.0$ . A given spectrum of fluctuations is applied at  $t = 0$ ; the simulation then follows the subsequent temporal evolution of the system. The fluctuating magnetic and electric fields initially imposed upon the system are:

$$\delta \mathbf{B}(x, t = 0) = \sum_{n=1}^{nmax} -\hat{\mathbf{y}} \delta B_n \sin(-k_n x + \phi_n) + \hat{\mathbf{z}} \delta B_n \cos(-k_n x + \phi_n) \quad (1)$$

$$\delta \mathbf{E}(x, t = 0) = \sum_{n=1}^{nmax} \hat{\mathbf{y}} \delta E_n \cos(-k_n x + \phi_n) + \hat{\mathbf{z}} \delta E_n \sin(-k_n x + \phi_n) \quad (2)$$

with  $\delta B_n$  as the amplitude of mode  $n$ ,  $\delta E_n = (\omega/kc)\delta B_n$ , and wavenumber  $k = k_{\parallel}$  understood. Each mode is a normal mode of the plasma with dispersion properties as given by solutions of the electromagnetic dispersion equation at  $\mathbf{k} \times \mathbf{B}_o = 0$  [Chapter 6, *Gary*, 1993]. Spatially inhomogeneous velocity perturbations are added to each particle component at  $t = 0$  to make the particles more nearly self-consistent with the field fluctuations of Equations (1) and (2).

The initial power spectrum is chosen to be

$$\frac{|\delta B(t=0)|^2}{B_o^2} = S_B \sum_{n=1}^{nmax} (k_n c / \omega_e)^{-\alpha} \quad (3)$$

with  $nmax = 30$  whistler modes which are equally spaced in wavenumber. We further chose  $\alpha = 3$  [*Smith et al.*, 2006],  $k_1 c / \omega_e = 0.153$ , and  $k_{30} c / \omega_e = 0.598$ , corresponding to the magnetosonic-whistler dispersion properties. We choose  $|\delta B(t=0)|^2 / B_o^2 = 0.01$ .

Although these modes are discrete, most have a nonzero damping decrement. This means that the resonant velocity factor of each mode has a finite width in  $v_{\parallel}$  [*Gary and Saito*, 2003]; the velocity overlap of these factors implies that electron scattering by this discrete fluctuation spectrum should emulate the consequences of scattering by the essentially continuous power spectrum of magnetic fluctuations in the solar wind.

Figure 4a shows the temporal evolution of the total fluctuating magnetic field energy for this simulation; there is a modest decrease in  $|\delta B|^2 / B_o^2$  with time, corresponding to the damping which transfers energy to the electrons, particularly the cyclotron resonant strahl. Figure 4b illustrates the initial and final power spectra of the fluctuations; as predicted by linear theory, the short wavelength modes have the strongest damping.

Figure 5 illustrates the electron velocity distribution  $f_e(v_{\parallel}, v_y)$  at  $t = 0$  and  $|\Omega_e|t = 100$ . Pitch-angle scattering of the strahl is evident; furthermore, the figure suggests that this scattering is greater at larger electron energies.

This suggestion is borne out by Figure 6 which shows electron pitch-angle distributions from this run at  $t = 0$  and at  $|\Omega_e|t = 100$  for three different values of  $v$ . At the start of the simulation, our choice of a bi-Maxwellian suprathermal velocity distribution corresponds to pitch-angle distributions which become narrower as  $|v_{\parallel}|$  increases. But at late times, the opposite trend is evident; clearly the whistlers have induced a broadening in pitch-angle with increasing electron energy.

#### 4. Conclusions and Interpretations

We have used particle-in-cell simulations to compute suprathermal electron responses to electromagnetic fluctuation spectra from two distinct sources: the whistler anisotropy

instability driven by  $T_{\perp}/T_{\parallel} > 1$  on the electron core component, and a broadband, decreasing power-law spectrum of whistler fluctuations imposed upon the system at  $t = 0$ . Both simulations show that such enhanced fluctuations lead to broadening of strahl pitch-angle distributions, providing further evidence that whistlers are a likely source of scattering for suprathermal electrons in the solar wind. But the two different whistler sources have distinctly different consequences.

The instability-driven fluctuations are enhanced over a narrow range of wave numbers which mainly scatters the low energy core electrons. Strahl electrons with velocities close to those of the core are also scattered and their pitch-angles are increased, but at higher energies the strahl retains its initial narrow character. Strahl pitch-angle distributions are often observed to become more narrow as electron energy increases (See citations above). Particle-particle collisions become weaker with increasing electron energy, and are a plausible source for this narrowing of the strahl. But *Lemons and Feldman* [1983] have shown that collisions are not always sufficient to describe the observed strahl width, especially at lower energies. Thus, scattering by enhanced fluctuations from the whistler anisotropy instability may also contribute to this characteristic strahl property. Because this instability reduces but does not necessarily eliminate the driving anisotropy, a residual  $T_{\perp c}/T_{\parallel c} > 1$  may be an observational indication that this growing mode has contributed to strahl broadening.

The initially-imposed broadband whistlers resonate with and scatter a broader range of strahl; because longer wavelength fluctuations have greater energies, they interact with the faster electrons more strongly, leading to distributions which become broader with increasing electron energy. We assume the breakpoint between the inertial range of solar wind MHD turbulence and the so-called “dissipation” range (or, more accurately, following *Stawicki et al.* [2001], the “dispersion” range) of whistler turbulence corresponds to  $k_{\parallel}c/\omega_p \simeq 1$ . If we further assume that this breakpoint corresponds to the onset of strong scattering to electron isotropy, then the corresponding electron energy at cyclotron resonance is  $m_e v_{\parallel}^2/2 \simeq (m_p/m_e)^2 (v_A/c)^2 (m_e c^2/2)$ . For typical solar wind parameters near 1 AU of  $B_o = 5$  nT and  $n_e = 5$  cm<sup>-3</sup>, this equation predicts that electrons above about 23 keV should be scattered to isotropy.

It would be good to carry out further such simulations to determine how suprathermal scattering changes with variations in relevant plasma parameters, as well as to facilitate comparison against observations. But publication constraints prevent such work from being described here.

**Acknowledgments.** The authors acknowledge useful discussions with Ruth Skoug and John Steinberg. This work was performed under the auspices of the U.S. Department of Energy (DOE) and was supported by the DREAM project of the Laboratory Directed Research and Development Program at Los Alamos, as well as the Sun-Earth Connection

Theory Program and the Solar & Heliospheric Physics SR&T Program of the National Aeronautics and Space Administration.

## References

Bale, S. D., P. J. Kellogg, F. S. Mozer, T. S. Horbury, and H. Reme (2005), Measurement of the electric fluctuation spectrum of magnetohydrodynamic turbulence, *Phys. Rev. Lett.*, *94*, 215002.

Beinroth, H. J., and F. M. Neubauer (1981), Properties of whistler mode waves between 0.3 and 1.0 AU from Helios observations, *J. Geophys. Res.*, *86*, 7755.

Buneman, O. (1993), Computer space plasma physics, in *Simulation Techniques and Software*, edited by H. Matsumoto and Y. Omura, P. 67, Terra Sci., Tokyo.

Feldman, W. C., J. R. Asbridge, S. J. Bame, M. D. Montgomery, and S. P. Gary (1975), Solar wind electrons, *J. Geophys. Res.*, *80*, 4181.

Feldman, W. C., J. R. Asbridge, S. J. Bame, J. T. Gosling, and D. S. Lemons (1978), Characteristic electron variations across simple high-speed solar wind streams, *J. Geophys. Res.*, *83*, 5285.

Gary, S. P. (1993), *Theory of Space Plasma Microinstabilities*, Cambridge University Press, New York.

Gary, S. P., and S. Saito (2003), Particle-in-cell simulations of Alfvén-cyclotron wave scattering; Proton velocity distributions, *J. Geophys. Res.*, *108*, 1194, doi:10.1029/2002JA009824.

Gary, S. P., and J. Wang (1996), Whistler instability: Electron anisotropy upper bound, *J. Geophys. Res.*, *101*, 10,749.

Gosling, J. T., R. M. Skoug, and W. C. Feldman (2001), Solar wind electron halo depletions at 90° pitch angle, *Geophys. Res. Lett.*, *28*, 4155.

Hammond, C. M., W. C. Feldman, D. J. McComas, J. L. Phillips, and R. J. Forsyth (1996), Variation of electron-strahl width in the high-speed solar wind: Ulysses observations, *Astron. Astrophys.*, *316*, 350.

Lemons, D. S., and W. C. Feldman (1983), Collisional modification to the exospheric theory of solar wind halo electron pitch angle distributions, *J. Geophys. Res.*, *88*, 6881.

Lengyel-Frey, D., R. A. Hess, R. J. MacDowall, R. G. Stone, N. Lin, A. Balogh, and R. Forsyth (1996), Ulysses observations of whistler waves at interplanetary shocks and in the solar wind, *J. Geophys. Res.*, *101*, 27,555.

Maksimovic, M., I. Zouganelis, J.-Y. Chaufray, K. Issautier, E. E. Scime, J. E. Littleton, E. Marsch, D. J. McComas, C. Salem, R. P. Lin, and H. Elliott (2005), Radial evolution of the electron distribution functions in the fast solar wind between 0.3 and 1.5 AU, *J. Geophys. Res.*, *110*, A09104, doi:10.1029/2005JA011119.

Pagel, C., N. U. Crooker, D. E. Larson, S. W. Kahler, and M. J. Owens (2005), Understanding electron heat flux signatures in the solar wind, *J. Geophys. Res.*, *110*, A01103, doi:10.1029/2004JA010767.

Pagel, C., S. P. Gary, C. A. de Koning, R. M. Skoug, and J. T. Steinberg (2006), Whistler scattering of suprathermal electrons in the solar wind, *J. Geophys. Res.*, submitted.

Phillips, J. L., and J. T. Gosling (1990), Radial evolution of solar wind thermal electron distributions due to expansion and collisions, *J. Geophys. Res.*, *95*, 4217, 1990.

Phillips, J. L., J. T. Gosling, D. J. McComas, S. J. Bame, and E. J. Smith (1989), ISEE 3 observations of solar wind thermal electrons with  $T_{\perp} > T_{\parallel}$ , *J. Geophys. Res.*, *94*, 13,377.

Pierre, F., J. Solomon, N. Cornilleau-Wehrin, P. Canu, E. E. Scime, J. L. Phillips, A. Balogh, and R. J. Forsyth [1995], Whistler-mode wave generation around interplanetary shocks in and out of the ecliptic plane, *Geophys. Res. Lett.*, *22*, 3425.

Pilipp, W. G., H. Miggenrieder, K.-H. Mühlhäuser, H. Rosenbauer, R. Schwenn, and F. M. Neubauer (1987), Variations of electron distribution functions in the solar wind, *J. Geophys. Res.*, *92*, 1103.

Rosenbauer, H., R. Schwenn, E. Marsch, B. Meyer, H. Miggenrieder, M. D. Montgomery, K. H. Mühlhäuser, W. Pilipp, W. Voges, and S. M. Zink (1977), A survey on initial results of the Helios plasma experiment, *J. Geophys.*, *42*, 561.

Smith, C. W., K. Hamilton, B. J. Vasquez, and R. J. Leamon (2006), Dependence of the dissipation range spectrum of interplanetary magnetic fluctuations on the rate of energy cascade, *Astrophys. J.*, *645*, L85.

Stawicki, O., S. P. Gary, and H. Li, Solar wind magnetic fluctuation spectra: Dispersion versus damping, *J. Geophys. Res.*, *106*, 8273, 2001.

Vocks, C., and G. Mann (2003), Generation of suprathermal electrons by resonant wave-particle interaction in the solar corona and wind, *Astrophys. J.*, *593*, 1134.

Vocks, C., C. Salem, R. P. Lin, and G. Mann (2005), Electron halo and strahl formation in the solar wind by resonant interactions with whistler waves, *Astrophys. J.*, *627*, 540.

## Figure Captions

**Figure 1.** Simulation results for the whistler anisotropy instability run. (a) The normalized magnetic fluctuation field energy density as a function of time and (b) the power spectrum of the fluctuating magnetic fields at  $|\Omega_e|t = 100$  as a function of the parallel wavenumber.

**Figure 2.** Simulation results for the whistler anisotropy instability run. The electron velocity distribution  $\log[f_e(v_{\parallel}, v_y)/f_e(0, 0)]$  at  $t = 0$  and at  $|\Omega_e|t = 100$  where  $v_{\parallel}$  and  $v_y$

are normalized by  $v_c$ , the core thermal speed.

**Figure 3.** Simulation results for the whistler anisotropy instability run. Electron pitch angle distributions at  $t = 0$  (dashed lines) and at  $|\Omega_e|t = 100$  (solid lines) for electrons with  $v^2 = 20v_c^2$ ,  $30v_c^2$ , and  $40v_c^2$  as labeled.

**Figure 4.** Simulation results for the run with an initially imposed spectrum of enhanced fluctuations. (a) The normalized magnetic fluctuation field energy density perpendicular to the background magnetic field as a function of time and (b) the power spectrum  $|(\delta B_n)_y|^2/|(\delta B_1)_y|^2$  at  $t = 0$  (solid dots) and at  $|\Omega_e|t = 100$  (open circles) as a function of the parallel wavenumber.

**Figure 5.** Simulation results for the run with an initially imposed spectrum of enhanced fluctuations. The electron velocity distribution  $\log[f_e(v_{\parallel}, v_y)/f_e(0, 0)]$  at  $t = 0$  and at  $|\Omega_e|t = 100$  where  $v_{\parallel}$  and  $v_y$  are normalized by  $v_c$ , the core thermal speed.

**Figure 6.** Simulation results for the run with an initially imposed spectrum of enhanced fluctuations. Electron pitch angle distributions at  $t = 0$  (dashed lines) and at  $|\Omega_e|t = 100$  (solid lines) for electrons with  $v^2 = 20v_c^2$ ,  $30v_c^2$ , and  $40v_c^2$  as labeled.

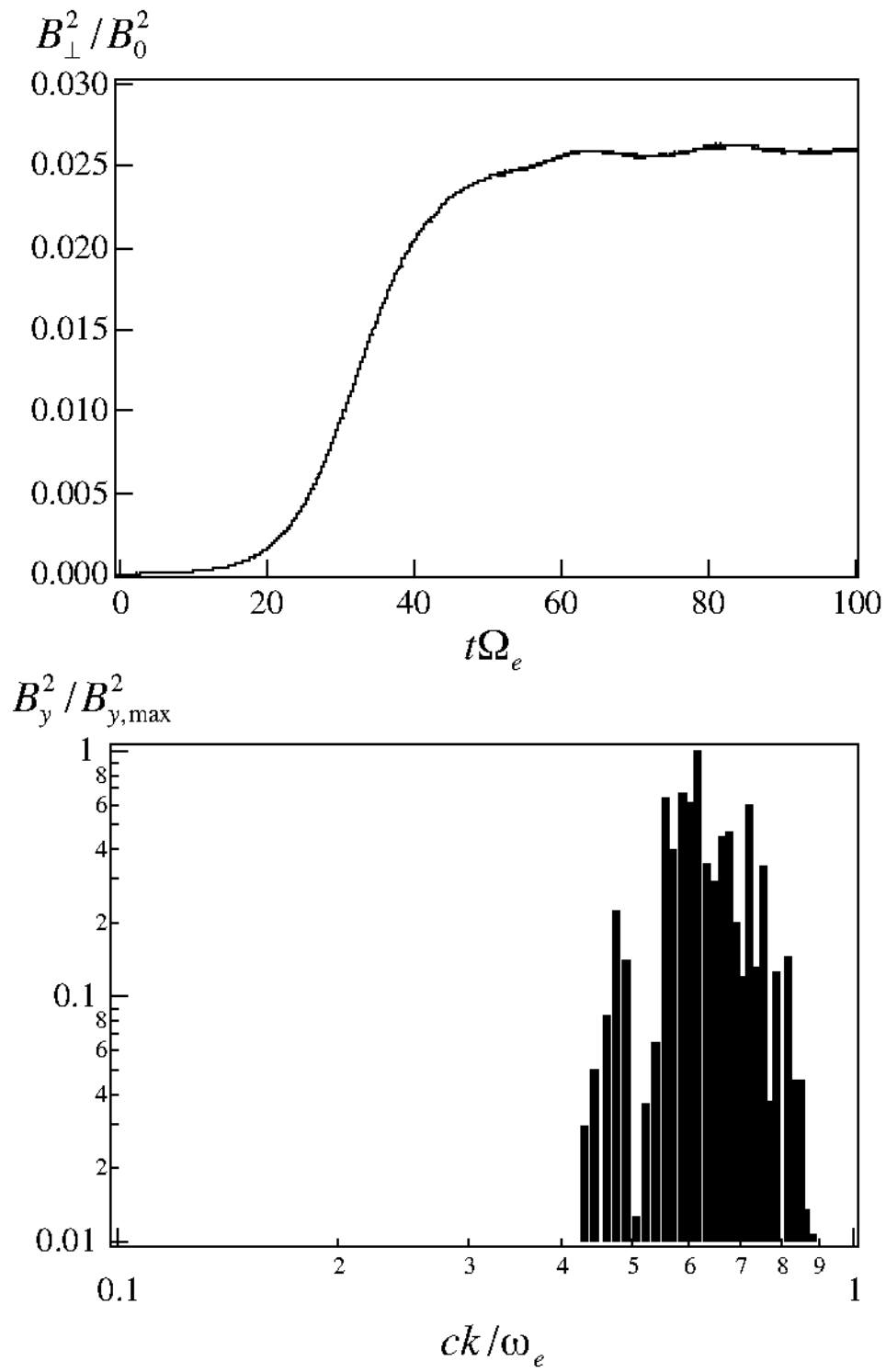


Figure 1

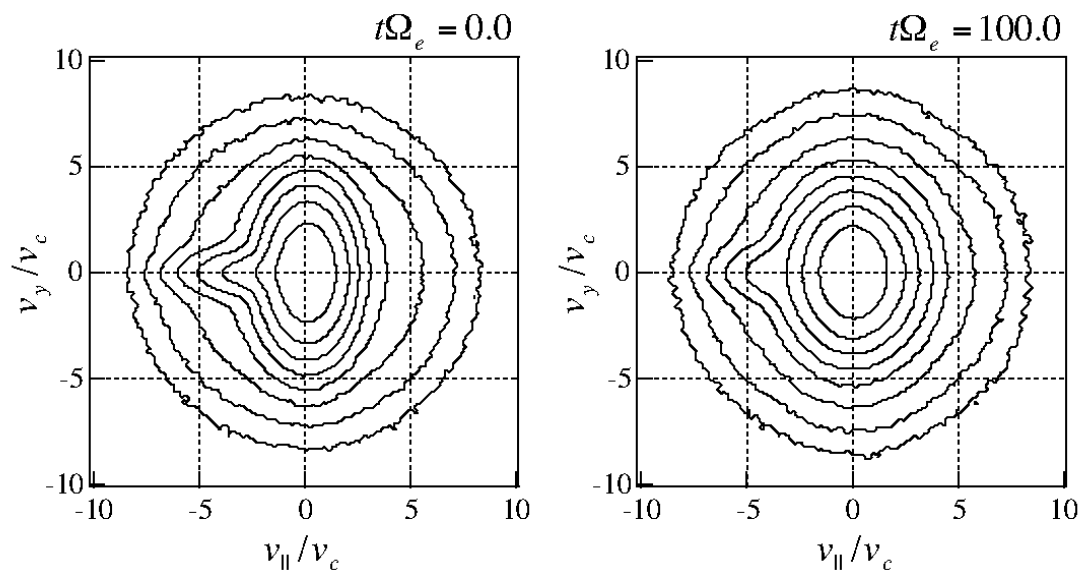


Figure 2

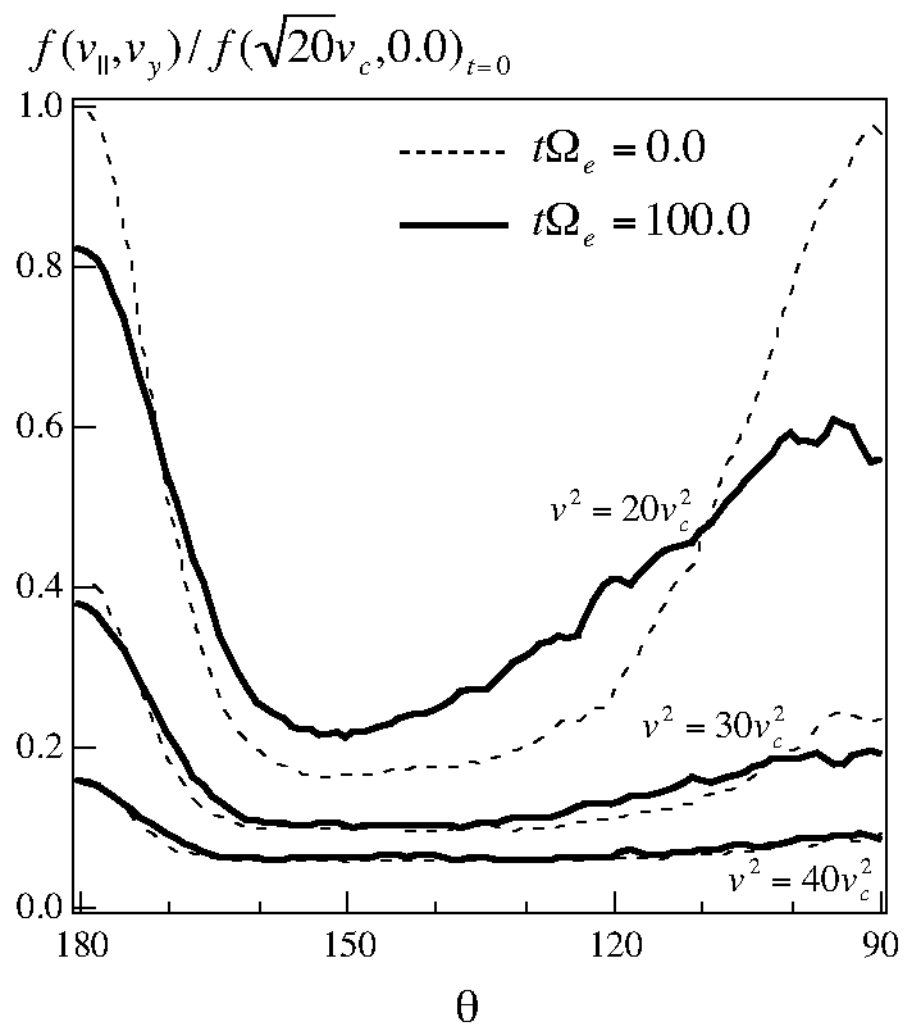


Figure 3

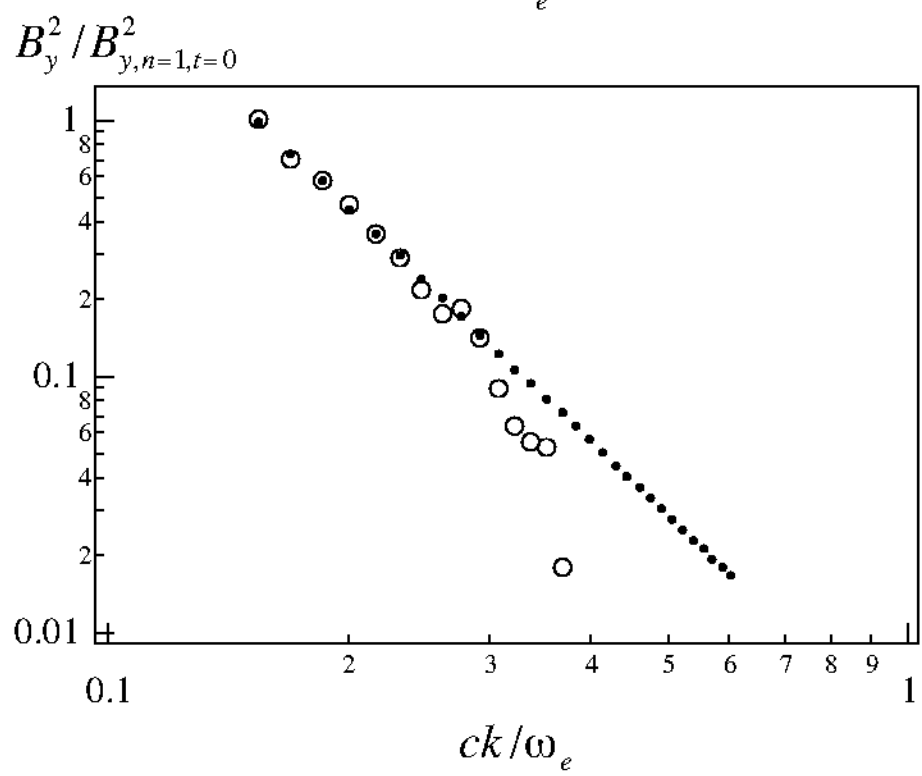
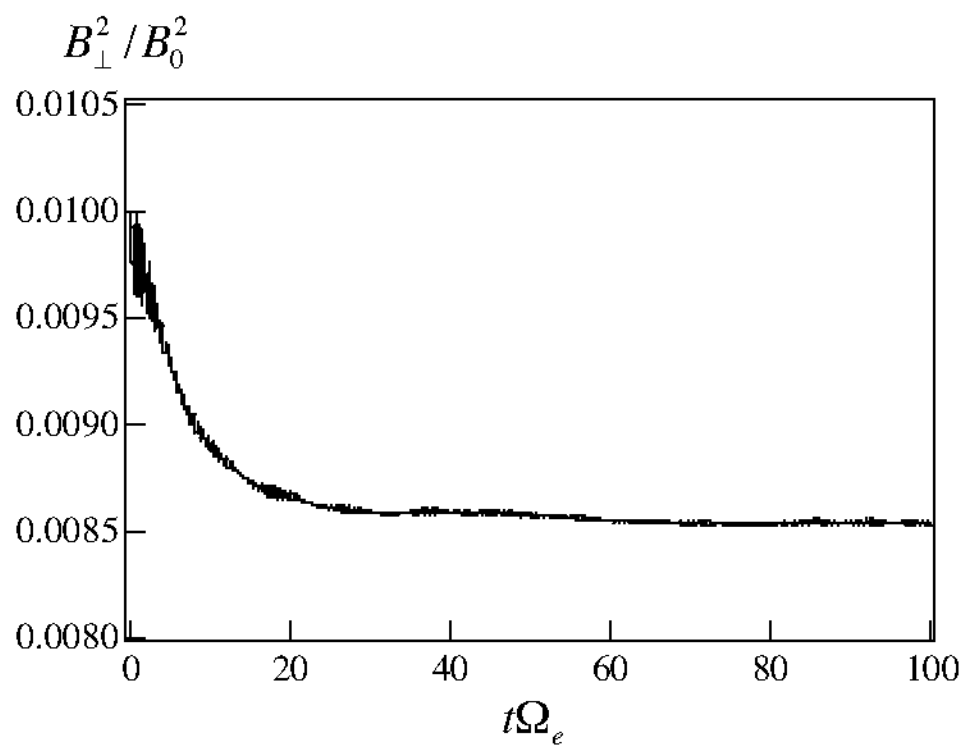


Figure 4

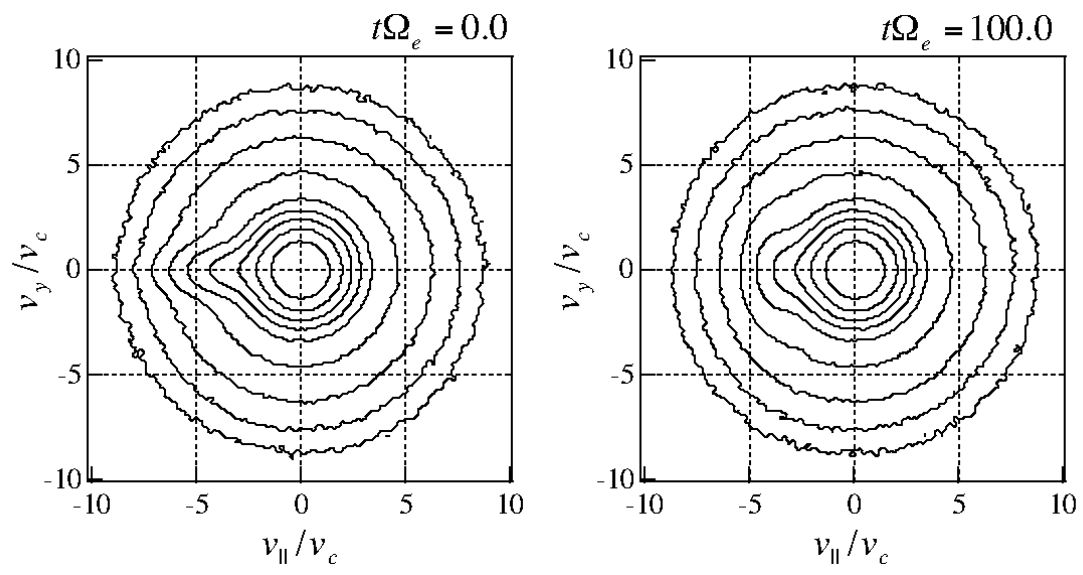


Figure 5

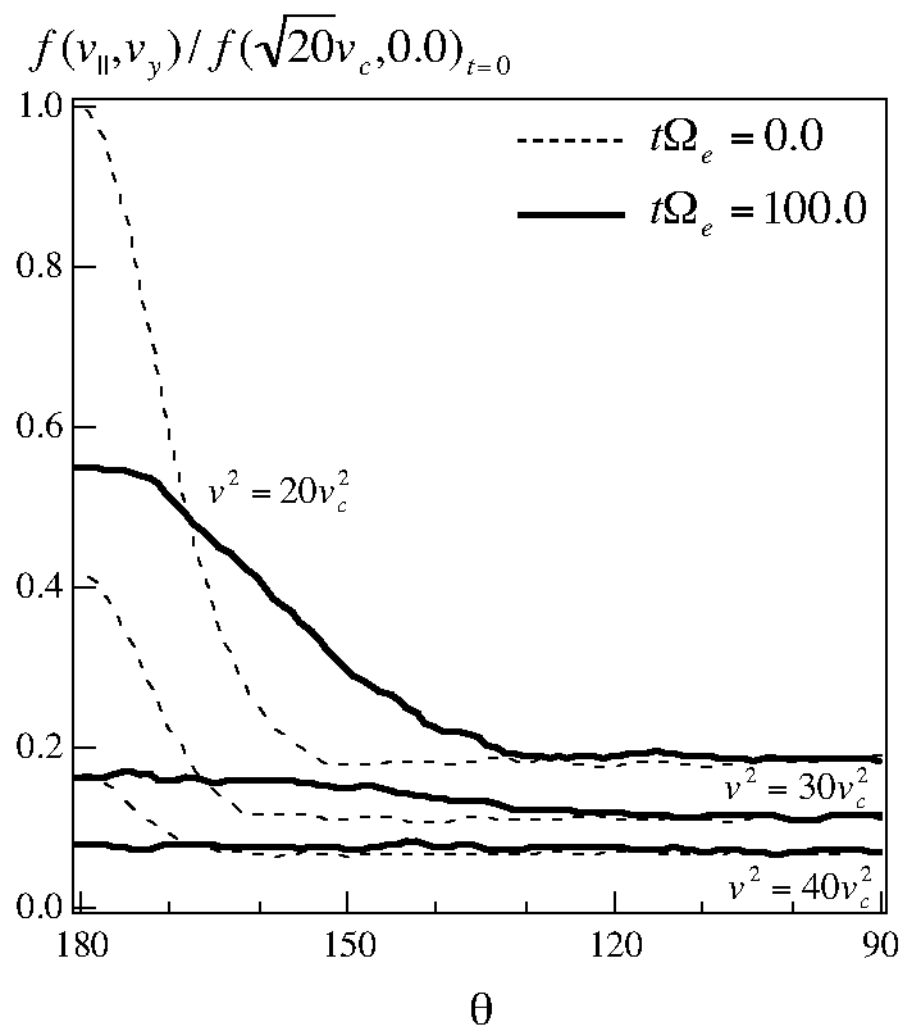


Figure 6